



Hartree-Fock, molecular docking, spectral, kinetic and antitumor considerations for cobalt, nickel, palladium and platinum (II)-bis carbothiohydrazone complexes



Nashwa M. El-Metwaly^{a,*}, Marwa G. El-Ghalban^b

^a Chemistry Department, College of Applied Sciences, Umm Al-Qura University, Makkah, Saudi Arabia

^b Chemistry Department, Faculty of Science, Mansoura University, Mansoura, Egypt

ARTICLE INFO

Article history:

Received 31 January 2016

Received in revised form 16 April 2016

Accepted 18 April 2016

Available online xxxx

Keywords:

Schiff base

Hartree-Fock

Molecular docking

Spectral

TEM

Antitumor

ABSTRACT

New metal ion complexes were synthesized using Schiff base derivative and characterized using spectral and theoretical analysis. IR and ¹H NMR spectra, suggest bi-dentate to tetra-dentate mode of bonding each towards two metal ions. Square-planar and octahedral configurations are the two proposed geometries for Pd(II) or Pt(II) and Co(II) or Ni(II) complexes, respectively. Significant spectral parameters were calculated to emphasize on the type of bonds between active sites and the metal atoms. XRD patterns and TEM images stressed on the nanometer sized appearance for all investigated compounds. Theoretical considerations were implemented using Gaussian09 and Autodock computational tools. HF/LANL2DZ molecular modeling exerts the optimized structures which agree with the spectral data. The frontier molecular orbitals, HOMO and LUMO were calculated. Also, the calculated geometric parameters foresee the distinguish bioactive features of all compounds under interest. Molecular docking utilizes defiant protein receptors attributed to the microorganisms executed in biological application as; 3t88, 3ty7, 3cku, 2ylh and 2jrs. Considerable reduction in binding energies was recorded along the docking process. The docked Schiff base ligand displays significant energy data with *hepatocellular carcinoma* (2jrs) and *Escherichia coli* (3t88) receptors. This deducts the affinity of designed drug against the two infections. The antibacterial and antifungal activities were tested against different microorganisms. The scanned compounds display a comparable inhibition activity along the investigation process. IC₅₀ was determined for all compounds against hepatocellular carcinoma cells. Co(II) and Ni(II) complexes are introducing an excellent activity towards the inhibition of all microorganisms and also offer the best IC₅₀ values in carcinoma cell line investigation.

© 2016 Elsevier B.V. All rights reserved.

1. Introduction

In the last few decades the Schiff base ligands include NSO donors have attracted the researcher insight to intensify the research dealing with such chelating compounds. Schiff base metal ion complexes are taken a great attention due to their enormous application in different areas based on the role of metal ion in enhancement the activity at all. Antitumor, antiaprotzoal and antibacterial activates are recorded with different thiosemicarbazone complexes [1–4]. A series of salicylaldehyde thiosemicarbazone complexes have been synthesized using Pd(II), Cu(II) and Ru(III) ions. The complexes isolated have 1:1 and 1:2 (M:L) molar ratios [5]. Also, vanadium complex was prepared from salicylaldehyde thiosemicarbazone and tri-dentate mode of bonding was proposed through ONS donors [6]. Generally, the divalent metal ion complexes have been used for the complexation towards diprotic Schiff base ligands with

N₂O₂ donors [7,8]. In continuation for previous work [9–15], here in our study we are dealing with bis derivative for thiocarbohydrazide with salicylaldehyde. The bis derivative includes multi-donor centers which enriches the coordination towards bivalent cobalt and nickel group metals. The spectral, thermal and kinetic studies will be used to establish the structural formula of the complexes. Gaussian09 molecular modeling and Autodock molecular docking will be elaborately implemented to serve the chemical and biological investigations.

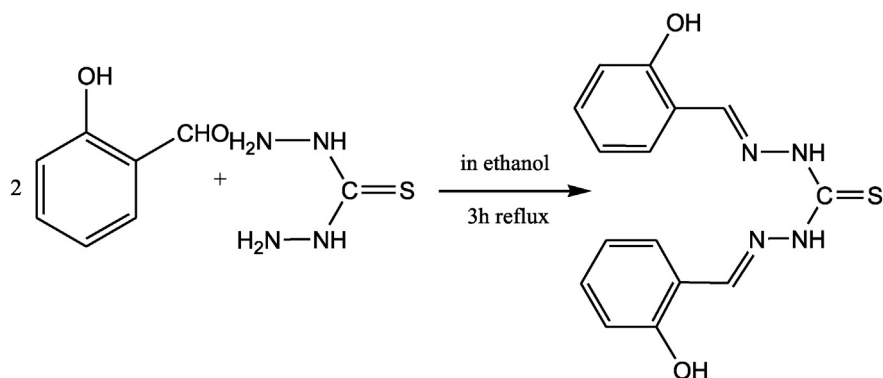
2. Experimental

2.1. Reagents

The chemicals concerned in this study to prepare the Schiff base ligand are, thiocarbohydrazide and salicylaldehyde were purchased from Fulka and employed as it is. Also, the metal chloride salts used for complexation as; CoCl₂(H₂O)₆, NiCl₂(H₂O)₆, PdCl₂ and, PtCl₂ are commercially available from Sigma-Aldrich. The solvents used in synthesis process are utilized without previous purification.

* Corresponding author.

E-mail address: n_elmetwaly00@yahoo.com (N.M. El-Metwaly).



Scheme 1. Synthesis of *N',2*-bis(*E*)-2-hydroxybenzylidene) hydrazine-1-carbothiohydrazide.

2.2. Synthesis

2.2.1. Synthesis of *N',2*-bis(*E*)-2-hydroxybenzylidene) hydrazine-1-carbothiohydrazide (H_3L)

In a round bottom flask, 1:2 M ratio from thiocarbonylhydrazide (5 mmol, 0.50 g) to salicylaldehyde (10 mmol, 1.722 g) is condensed in ethanolic solution (40 mL) (Scheme 1). The mixture was refluxed for ≈ 3 h, allowed to cool down. The yellow precipitate Schiff base product was collected by filtration, washed with ether and re-crystallized in ethanol by a suitable yield (65%). The elemental analyses are; C; 57.36 (calcd. 57.30%), H; 4.48 (calcd. 4.49%) and N; 18.83 (calcd. 17.82%). The structural formula of the ligand ($C_{15}H_{14}N_4O_2S$) was verified by spectral analysis.

2.2.2. Synthesis of metal ion complexes

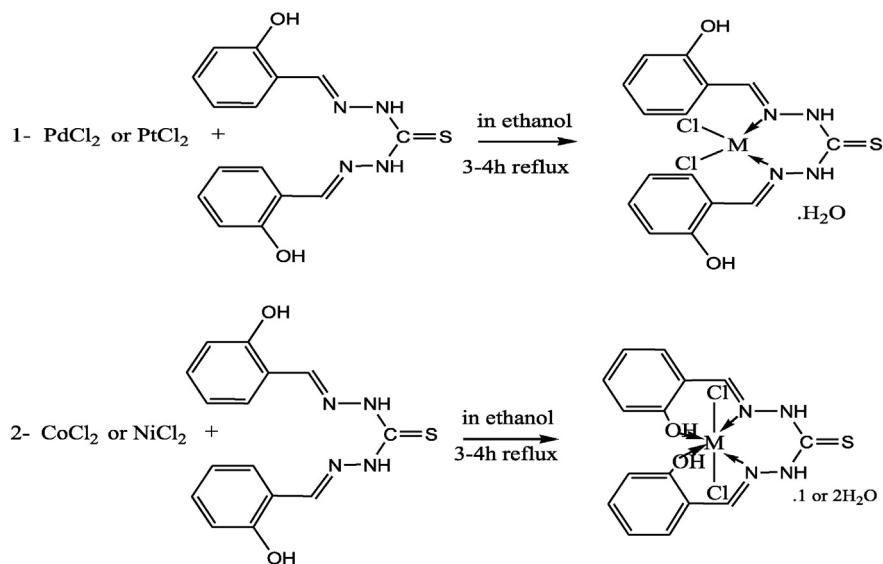
The synthesis process were carried out (Scheme 2) at the same conditions except the Co(II) complex. The precipitation of Co(II) complex needs

few drops of tri-ethylamine to accelerate the reaction which sometimes distinguish cobalt complexation. Equi-molar ratios (1:1) were mixed from Schiff base ligand to each metal salt. 0.3144 g (1 mmol) of ligand dissolved in ethanol, was added drop wisely to metal chloride solution attributed to, $CoCl_2(H_2O)_6$ (0.238 g); $NiCl_2(H_2O)_6$ (0.238 g); $PdCl_2$ (0.177 g) and $PtCl_2$ (0.266 g). The mixtures refluxed for 3–4 h, the precipitates were filtered off washed with ethanol, diethyl ether and finally dried in a vacuum desiccator.

2.3. Biological activity

2.3.1. Anti-microorganisms activity

The compounds under investigation were tested individually against bacteria, *Escherichia coli* (G^-) and *Staphylococcus aureus* (G^+) and fungi as; *Aspergillus fumigatus* and *canadida albicans*. The biological investigation was implemented using agar well diffusion methods



Scheme 2. The synthesis process of complexes.

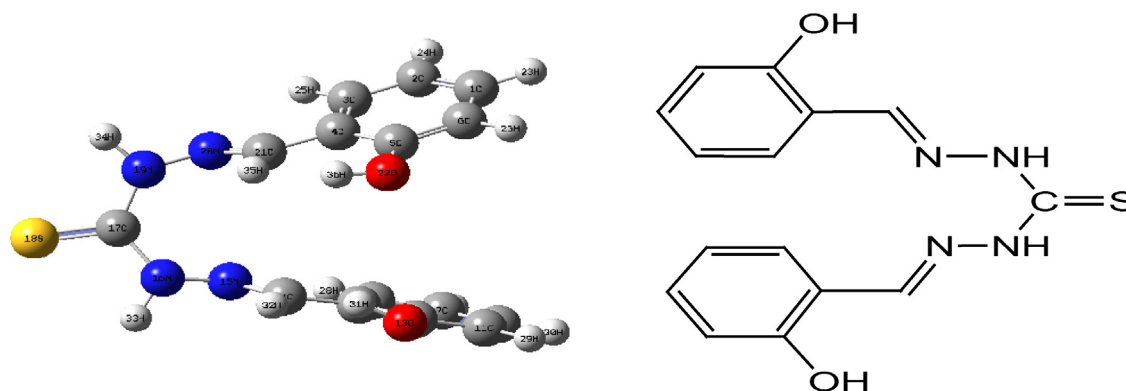
Table 1

Analytical and physical data of H_3L Schiff base ligand and its metal complexes.

Compound empirical formula (Calcd)	Color	Elemental analysis (%) Calcd/Found				
		C	H	N	M	Cl
1) $[C_{15}H_{14}N_4O_2S]$ (314.35)	Yellow	57.30/57.36	4.49/4.48	17.82/17.83	–	–
2) $[Co(Cl)_2(C_{15}H_{14}N_4O_2S)](H_2O)$ (462.21)	Brown	38.98/38.99	3.49/3.52	12.12/12.14	12.75/12.80	15.34/15.44
3) $[Ni(Cl)_2(C_{15}H_{14}N_4O_2S)](H_2O)_2$ (479.97)	Dark green	37.54/37.8	3.78/3.77	11.67/11.64	12.23/12.22	14.77/14.55
4) $[Pd(Cl)_2(C_{15}H_{14}N_4O_2S)](H_2O)$ (509.69)	Orange	35.35/35.40	3.16/3.20	10.99/11.10	20.88/20.87	13.91/13.92
5) $[Pt(Cl)_2(C_{15}H_{14}N_4O_2S)](H_2O)$ (598.34)	Brownish yellow	30.11/30.13	2.69/2.67	9.36/9.40	32.60/32.61	11.85/11.88

Table 2Assignments of the IR spectral bands (cm^{-1}) of H_3L Schiff base and its metal complexes.

Compound	ν_{OH}	δ_{OH}	δ_{NH}	ν_{CN}	$\delta_{\text{r}}(\text{H}_2\text{O}), \delta_{\text{w}}(\text{H}_2\text{O})$	$\nu_{\text{C-O}}$	$\nu_{\text{CS(IV)}}$	$\nu_{\text{M-O}}$	$\nu_{\text{M-N}}$
1) $[\text{C}_{15}\text{H}_{14}\text{N}_4\text{O}_2\text{S}]$	3336	1399	1539	1595	–	1034	820	–	–
2) $[\text{Co}(\text{Cl})_2(\text{C}_{15}\text{H}_{14}\text{N}_4\text{O}_2\text{S})](\text{H}_2\text{O})$	3555	1380	1535	1535	850,650	1027	828	533	425
3) $[\text{Ni}(\text{Cl})_2(\text{C}_{15}\text{H}_{14}\text{N}_4\text{O}_2\text{S})](\text{H}_2\text{O})_2$	3415	1349	1543	1581	856, 670	1036	817	537	464
4) $[\text{Pd}(\text{Cl})_2(\text{C}_{15}\text{H}_{14}\text{N}_4\text{O}_2\text{S})](\text{H}_2\text{O})$	3424	1392	1536	1580	856,645	1038	820	–	460
5) $[\text{Pt}(\text{Cl})_2(\text{C}_{15}\text{H}_{14}\text{N}_4\text{O}_2\text{S})](\text{H}_2\text{O})$	3443	1399	1539	1578	850,660	1034	820	–	421

**Fig. 1.** The structural and optimized form of $N',2$ -bis(E)-2-hydroxybenzylidene) hydrazine-1-carbothiohydrazide (H_3L) ligand.

[16], pathological bacteria (1×10^6 CFU/mL) and (1×10^4 spore/mL) fungi were spread over nutrient agar (NA), Sab-dextrose agar and (SDA), respectively. After cooling the media will be solidified, 100 μl from tested compound were spread over 6 mm diameter. The solution was prepared by dissolving 20 mg of the compound in DMSO solvent. The plates were then impregnated for 24 h, 37 $^\circ\text{C}$ and 48 h, 28 $^\circ\text{C}$ for bacteria and fungi, respectively. The control was prepared using DMSO solvent employed in investigation. Ampicillin (50 $\mu\text{g}/\text{mL}$), and Amphotericin B (50 $\mu\text{g}/\text{mL}$) were utilized as referenced bacteria and fungi, respectively. After impregnation, the activity was evaluated by measuring the inhibition zone in comparing with the reference as millimeters expressing the mean values for triplicate.

2.3.2. Antitumor activity

The cell lines were obtained from the American type culture collection (ATCC, Rockville, MD). The cells were grown on RPMI-1640 medium supplemented with 10% inactivated fetal calf serum and 50 $\mu\text{g}/\text{L}$ gentamycin. The cells were maintained at 37 $^\circ\text{C}$ in humidified atmosphere with 5% CO_2 and were sub-cultured two to three times a week. Briefly, the cell lines were grown as mono layers in growth mediums. The minelayers of 10,000 cells adhered at the bottom of the wells in a 96-well microtiter plate (Falcon, NJ, USA) promoted for 24 h at 37 $^\circ\text{C}$ in a humidified incubator with 5% CO_2 . The monolayer were then washed with sterile phosphate buffered saline (0.01 M pH 7.2) and simultaneously the cells were treated with 100 μL from different dilutions of tested compounds in fresh maintenance medium and incubated at 37 $^\circ\text{C}$. A control of untreated cells was made in the absence of the tested compounds. Three wells were used from each concentration for tested samples. Every 24 h the observation under inverted microscope was made. The number of the surviving cells was determined by staining the cells with crystal violet followed by cell lysing using 33% glacial acetic acid and read the absorbance at 590 nm using ELISA reader after well mixing. The absorbance values from untreated cells were considered as 100% proliferation and the percentage of availability was calculated as $(1 - \text{ODT} / \text{ODC}) * 100\%$ where ODT is the mean optical density of the wells treated with the tested compounds and ODC is the mean optical density of untreated cells [17–19].

2.4. Equipments

Carbon, H and N were analyzed at the Microanalytical unit of Cairo University. The metal and chloride contents were determined using slandered methods [20]. The molar conductivities of freshly prepared 1.0×10^{-3} mol/ cm^3 DMSO solutions were measured for the soluble complexes using Jenway 4010 conductivity meter. The X-ray diffraction patterns (XRD) were obtained on Pikagu diffractometer using $\text{CuK}\alpha$ radiation. Transmittance electron microscopy (TEM) images were taken in Joel JSM-6390 equipment. The infrared spectra, as KBr discs, were recorded on JASCO FT-IR-4100 Spectrophotometer ($400\text{--}4000$ cm^{-1}). The electronic and ^1H NMR (200 MHz) spectra were recorded on UV₂ Unicam UV/Vis, and a Varian Gemini Spectrophotometers. The effective magnetic moments were evaluated at room temperature by applying $\mu_{\text{eff}} = 2.828 \sqrt{X_M T}$, where X_M is the molar susceptibility corrected using Pascal's constants for the diamagnetism of all atoms in the ligand using a Johnson Matthey magnetic susceptibility balance. The thermal analysis was carried out on a Shimadzu thermogravimetric analyzer at a heating rate of 10 $^\circ\text{C min}^{-1}$ under nitrogen (20–900 $^\circ\text{C}$ range). The biological activity was evaluated at the Regional center for Mycology and biotechnology, Al-Azhar University, Cairo, Egypt.

2.5. Theoretical calculations

2.5.1. Kinetic studies

The kinetic parameters assigned to thermal analysis were calculated. The order (n) and the energy of activation (E) of suitable decomposition stages were determined for TG curves. Formerly, different researchers

Table 3 ^1H NMR data for the ligand and some of its complexes.

δ (ppm)	H_3L	$\text{Pd(II)-H}_3\text{L}$	$\text{Pt(II)-H}_3\text{L}$
M, 8H, Ph	7.88–7.95	7.1–8.21	7.23–7.61
S, 2H, 2CHN	7.59 and 7.62	9.14 and 9.16	7.88 and 7.95
S, 2H, 2OH	12.05	12.06	12
DMSO + H_2O	3.3	3.85	3.66
S, 2H, 2NH	2.5	2.49	2.5

Table 4
The spectroscopic, covalence parameters and magnetic moments of complexes.

2, 3	ν_2 (cm ⁻¹)	* ϵ_2	$10^{5**}f_2$	ν_3 (cm ⁻¹)	ϵ_3	10^5f_3	f_3/f_2	μ_{eff} (BM)	10Dq	B (cm ⁻¹)	β	Z
4, 5	ν_1 (cm ⁻¹)	* ϵ_1	$10^{5**}f_1$	ν_2 (cm ⁻¹)	ϵ_2	10^5f_2	f_2/f_1					
2)	16,666	110	1818	18,518	101	1794.5	0.99	4.14	8735	794.1	0.818	+1.103
3)	16,600	108	8942.4	25,600	91	8694	0.97	2.43	11,218	560.9	0.539	-0.256
4)	20,000	130	1375.4	22,727	280	1288	0.94	0				
5)	19,048	90	4140	22,222	70	3980	0.96	0				

*Molar absorptivity, **Oscillator strengths, f , calculated using the following expression: $f = 4.6 \times 10^{-9} \epsilon_{\text{max}} \nu_{1/2}$, where, ϵ_{max} is the molar absorptivity of the band maximum and $\nu_{1/2}$ is the band width at half-height expressed in wave numbers; C. J. Ballhausen, Prog. Inorg. Chem. 2.251(1960).

[21–29] were established equations and discussing their advantages. The rate of decomposition is the product of two separate functions of temperature and conversion using:

$$\frac{d\alpha}{dt} = k(T)f(\alpha) \quad (1)$$

where, α is the fraction decomposed at time t , $k(T)$ is the temperature dependent function and $f(\alpha)$ is the conversion function. The rate constant and dependent function $k(T)$ is of Arrhenius type.

$$K = Ae^{-E^*/RT} \quad (2)$$

where R , is the gas constant in (J mol⁻¹ k⁻¹) substituting Eq. (2) into Eq. (1) we get this equation

$$\frac{d\alpha}{dT} = \left(\frac{A}{\varphi e^{-E^*/RT}} \right) f(\alpha) \quad (3)$$

where φ , is the linear heating rate (dT/dt). From the integration and approximation, this equation can be obtained in the following form:

$$\ln g(\alpha) = \frac{-E^*}{RT} + \ln \left[\frac{AR}{\varphi E^*} \right] \quad (4)$$

where $g(\alpha)$ is a function depending on the mechanism of the reaction. The right hand side is known as temperature integral and has no close for solution. So, several techniques have been used to evaluate the temperature integral. The kinetic parameters for the ligand and its complexes are evaluated using Coat-Redfern [23] and Horowitz-Metzger methods [28].

2.5.2. Modeling methodology

The geometry of Schiff base ligand and its complexes are fully optimized by Hartree-Fock (HF) method with LANL2DZ base set using Gaussian09 software [30]. Gaussian output files were visualized by means of Gauss-View molecular visualization program [31]. In gas phase, according to the numbering scheme given in the view of the compounds, HF/quantum chemical parameters of the compounds are calculated from HOMO–LUMO energies. Also, bond lengths and effective charges for coordinating groups in optimized structures will be deducted.

Table 5
XRD spectral data of H₃L ligand and its complexes.

Compound	Size (nm)	θ	Intensity	d-Spacing (Å)	FWHM
H ₃ L	3.69	7.4	1000	5.979	0.396
Co(II)-H ₃ L	3.09	8.51	1010	5.208	0.474
Ni(II)-H ₃ L	3.77	13.08	1050	3.405	0.395
Pd(II)-H ₃ L	3.24	13.48	850	3.304	0.460
Pt(II)-H ₃ L	13.79	7.44	1000	6.325	0.106

2.5.3. Molecular docking

Docking calculations using Gasteiger partial charges added to the ligand (designed drug) atoms, were carried out using Autodock tools 4.2. Non-polar hydrogen atoms were conjoined, and rotatable bonds were illustrated. The calculations were performed on the ligand-protein pattern. Auto Dock tools were implemented after the addition of; fundamental hydrogen atoms, Kollman united atom type charges and salvation parameters [32]. Affinity (grid) maps of $\times \times$ Å grid points and 0.375 Å spacing were created applying the Autogrid program [33]. Calculating Vander Waals and the electrostatic terms were carried out using Auto Dock parameter set- and distance-dependent dielectric functions, respectively. Docking simulations were executed using the Solis & Wets local search method and the Lamarckian genetic algorithm (LGA) [34]. Initial position, orientation, and torsions of the ligand molecules were set indiscriminately. All rotatable torsions were emitted during docking. Each docking experiment was derived from 10 different runs that were set to close after a maximum of 250,000 energy assessments. The population size was set to 150. During the search, a translational step of 0.2 Å, and quaternion and torsion steps of 5 were applied.

3. Results and discussion

3.1. General

The basic analytical and physical data for Schiff base ligand and its Co(II), Ni(II), Pd(II) and Pt(II) complexes are tabulated (Table 1). All the investigated complexes are stable in air, having high melting points, insoluble in all organic solvents except DMSO and DMF are completely soluble. 1:1 (M:L) molar ratio is the general formula proposed for all investigated complexes. The molar conductivity measurements for 1 mmol/L in DMSO solvent represent 6.5–12.1 Ω^{-1} cm² mol⁻¹ values.

Table 6
Thermogravimetric analysis data for investigated compounds.

Complex	Steps	Temp. range/°C	Decomposed	Weight loss/Found (Calcd. %)
(1)	1st	43.69–310	-CH ₂ N ₂	13.41 (13.37)
	2nd	310–426.3	-(C ₇ H ₅ SO)	44.02 (43.74)
	3rd	426.3–550	-(C ₃ H ₇ N ₂ O)	27.34 (27.71)
	Residue		4C	15.23 (15.28)
(2)	1st	47.5–175.9	-H ₂ O	3.73 (3.89)
	2nd	176.9–400	-Cl ₂ + (C ₈ H ₇ N ₂)	43.70 (43.72)
	3rd	400.1–600	-(C ₇ H ₇ N ₂ S)	32.59 (32.72)
	Residue		CoO ₂	19.98 (19.67)
(3)	1st	42.6–283	-2H ₂ O + CH ₂ N ₂ + Cl ₂	30.66 (31.04)
	2nd	283–350.1	-(C ₈ H ₇ N ₂ OS)	37.1 (37.33)
	3rd	350.1–570	-(C ₆ H ₅ O)	19.67 (19.40)
	Residue		Ni	12.57 (12.23)
(4)	1st	24.1–420.1	-H ₂ O + C ₇ H ₆ NO + Cl ₂	41.05 (40.88)
	2nd	420.1–750.2	-(C ₈ H ₇ N ₂ O)	38.11 (37.98)
	Residue		Pd	20.88 (21.14)
(5)	1st	21.6–296.5	-(C ₁₀ H ₁₃ N ₃ O ₂) + H ₂ O + Cl ₂	48.97 (49.49)
	2nd	296.6–579	-(HCNS)	9.83 (9.88)
	Residue		Pt + 4C	41.20 (40.63)

Table 7Kinetic parameters using Coats–Red fern (CR) and Horowitz–Metzger (HM) operated for H₃L ligands and its complexes.

Comp.	Step	Method	Kinetic parameters					
			E (J mol ⁻¹)	A (S ⁻¹)	ΔS (J mol ⁻¹ K ⁻¹)	ΔH (J mol ⁻¹)	ΔG (J mol ⁻¹)	r
(1)	2nd	CR	1.39E + 05	8.94E - 02	-2.71E + 02	1.33E + 05	3.03E + 05	0.9993
		HM	1.56E + 05	1.53E + 11	-3.69E + 01	1.51E + 05	1.74E + 05	0.9991
(2)	3rd	CR	1.15E + 05	1.29E - 02	-2.89E + 02	1.09E + 05	3.40E + 05	0.9993
		HM	1.30E + 05	1.91E + 06	-1.33E + 02	1.23E + 05	2.29E + 05	0.9991
(3)	2nd	CR	7.85E + 04	2.06E - 02	-2.83E + 02	7.35E + 04	2.45E + 05	0.9993
		HM	9.53E + 04	1.22E + 06	-1.34E + 02	9.03E + 04	1.72E + 05	0.9991
(4)	2nd	CR	9.45E + 04	5.00E - 03	-2.98E + 02	8.75E + 04	3.36E + 05	0.9993
		HM	1.30E + 05	8.15E + 05	-1.40E + 02	1.23E + 05	2.40E + 05	0.9991
(5)	2nd	CR	1.31E + 05	3.98E - 02	-2.78E + 02	1.25E + 05	3.05E + 05	0.9993
		HM	1.58E + 05	6.85E + 10	-4.39E + 01	1.53E + 05	1.81E + 05	0.9991

These results display non-conducting features of the complexes [35]. This is expected with chloride anion which favor its covalent attachment with the metal ions.

3.2. IR and 1H NMR

All essential vibration bands of the ligand and its complexes are listed in Table 2. The ligand spectrum displays the following bands: 3336, 1399, 1595, 1034 and 820 cm⁻¹ assigned for νOH, δOH, δNH, νC=N and νC=S(IV), respectively [36]. The 1H NMR spectrum of the ligand (Table 3) (Fig. 1S) also displays peaks attributed to the protons in the configuration of thione tautomer form (Fig. 1) The comparative study for the IR spectra represents the significant unchangeable appearance for νC=S(I–IV), νNH and δNH bands. This proposed the exclusion of these groups from coordination towards the metal ions. This will be verified theoretically based on the optimizes stereo for sites distribution. The lower shift observed for νC=N band in the Co(II), Ni(II), Pd(II) and Pt(II) spectra shows the first coordination site in the sphere. Chloride anions are considered the integral part of complex sphere due to its coordination towards the central atoms. This proposal is in agreement with the anion gravimetric analysis and the non-conducting feature. The significant shift observed for νOH and δOH bands in [Co(Cl)₂(C₁₅H₁₄N₄O₂S)](H₂O) and [Ni(Cl)₂(C₁₅H₁₄N₄O₂S)](H₂O)₂ complexes, introduces the hydroxyl groups as the other coordination sites with the two metal ions. This is supported by the appearance of νM–O band at ≈530 cm⁻¹. While, the νOH band suffering the decline to high wave numbers, promote the presence of intra-ligand H-bonding before the complexation process which destroyed after that. So, the ligand mode of coordination with the [Pd(Cl)₂(C₁₅H₁₄N₄O₂S)](H₂O) and [Pt(Cl)₂(C₁₅H₁₄N₄O₂S)](H₂O) complexes as a neutral bi-dentate through the azomethine groups. While, the mode is changed to neutral tetra-dentate with Co(II) and Ni(II) ions. The neutrality feature of the ligand at all is expected behavior with chloride salts. The spectra of all complexes display a broad surround the range of 3440–3100 cm⁻¹, which could be attributed to the presence of solvent molecules [37]. These molecules may be physically or chemically attached with the metal ions. The crystal water appears at frequencies higher than that of the coordination. Therefore, the vibration modes range (3420–3370 cm⁻¹) considered a clear guide for the presence of lattice solvent. The chosen solvent proposed mainly based on the analytical, thermal and 1H NMR studies. The bands observed in

complexes spectra at 856 and ≈656 cm⁻¹ assign to δr (H₂O) and δw (H₂O) [38]. Also, the appearance of vibration bands attributed to the metallic bonds for νM–N in spectra supports all the previous data suggesting the mode of coordination. The inability to assign νM–Cl band due to the range of its appearance is out of the scan range. The 1H NMR spectra of [Pd(Cl)₂(C₁₅H₁₄N₄O₂S)](H₂O) (Fig. 1S) and [Pt(Cl)₂(C₁₅H₁₄N₄O₂S)](H₂O) complexes are confirming the data abstracted from IR. The down shift for the azomethine proton is suggesting the contribution of its nitrogen site. Also, more or less unshifted OH peak supports its ruling out. (See Table 3.)

3.3. Electronic spectra and magnetic measurements

The significant electronic spectral data and the magnetic moments are reported in Table 4. All the complexes spectra and their corresponding ligand were recorded in DMSO solvent with the absence of any changes during dissolution. The ligand spectrum recorded for 5.2 mmol/l shows bands at 31,250 and 27,777 cm⁻¹ for π → π* and 25,000 cm⁻¹ for n → π* intra-ligand transitions. The molar absorptivity values are, ε₁ = 226.9, ε₂ = 211.5 and ε₃ = 134.6 mol⁻¹ dm cm⁻¹. The high values are completely attached with the intra-ligand transition bands especially with π → π* transitions. The high conjugation for chromophor groups in the ligand form affecting on the position of charge transfer bands which nearby the visible region and deepen the color of the compound. Such molar absorptivity values were elevated with 3.3 mmol/l complex solution. This may refer to the presence of d-d transitions which have high oscillator strength values especially for the introductory transition step. The spectrum of [Co(Cl)₂(C₁₅H₁₄N₄O₂S)](H₂O) complex, exhibits two bands at 16,666 and 18,518 cm⁻¹ assign to 4T_{1g} → 4A_{2g} (ν₂) and 4T_{1g} → 4T_{1g} (p) (ν₃) transitions, respectively. The calculated spectral parameters values (10Dq, B and β) (Table 4) are within the reported range for octahedral geometry (Fig. 2). The high β value (0.818) indicates the ionic interaction with coordinating sites. The subnormal magnetic moment value (4.14 BM) point to the presence of strong M–M interaction or a strong L → M charge transfer transition. Moreover, the low magnetic moment value (2.53BM) of [Ni(Cl)₂(C₁₅H₁₄N₄O₂S)](H₂O)₂ complex in agreement with Co(II) complex appearance reflects the same assumption. The Ni(II) complex spectrum displays two bands at 25,600 and 16,600 cm⁻¹. These bands are attributing to 3A_{2g} → 3T_{1g} (p) (ν₃) and 3A_{2g} → 3T_{1g} (F) (ν₂)

Table 8

The Hartree-Fock parameters calculated for the ligand and its complexes.

Compound	E _H (eV)	EL (eV)	(EH-EL) (eV)	EL-Eh	X (eV)	μ (eV)	η (eV)	S (eV-1)	ω (eV)	ϕ (eV)
L	-0.21046	-0.08773	-0.1227	0.12273	0.149095	-0.1491	0.061365	0.030683	0.181124	16.29593416
Co	-0.31544	-0.09374	-0.2217	0.2217	0.20459	-0.20459	0.11085	0.055425	0.1888	9.02119982
Ni	-0.22712	-0.01039	-0.2167	0.21673	0.118755	-0.11876	0.108365	0.054183	0.065071	9.228071794
Pd	-0.31792	-0.16711	-0.1508	0.15081	0.242515	-0.24252	0.075405	0.037703	0.389984	13.26172005
Pt	-0.31378	-0.09601	-0.2178	0.21777	0.204895	-0.2049	0.108885	0.054443	0.192781	9.184001469

Table 9
Significant bond distances (Å) and dipole moment (Debye) of H₃L ligand with its complexes.

	CN ¹⁵	CN ²⁰	13O–C	22O–C	M–N ¹⁵	M–N ²⁰	M–O ¹³	M–O ²²	Dipole moment
1,4,5	CN ¹⁴	CN ¹⁹	21O–C	22O–C	M–N ¹⁴	M–N ¹⁹	M–O ²¹	M–O ²²	
1)	1.28024	1.279270	1.363189	1.363025	–	–	–	–	5.4067
2)	1.28744	1.280491	1.363221	1.363098	5.457591	4.875687	6.201717	6.226970	12.1226
3)	1.44181	1.356362	1.36391	1.36310	3.053270	2.846109	3.838932	3.584711	7.8208
4)	1.28199	1.280228	1.36304	1.36301	5.213593	4.884031	–	–	2.2841
5)	1.28031	1.280206	1.36301	1.36301	5.213593	4.884031	–	–	2.9709

transitions, respectively in an octahedral geometry (Fig. 2). The lower energy shift for d-d transitions is attached with bulk ligands, which perhaps introduce weak coordination [39]. The spectral parameters (10Dq, B and β) are also calculated [40]. The values are found to be 11,218, 560.9 and 0.539. The 10Dq value is found within the range of 3A_{2g} → 3T_{2g} (F) (ν_1) transition. The β value indicates high covalent interaction of sites which convenient with known NiN₆ and NiO₆ structures [41]. Generally, the shortage in β value is strongly associated with the reduction in the effective positive charge of central atom [42]. The Racah inter-electronic repulsion parameter values are varied for 3d transition metal complexes with changing Z and q values. Whereas, Z is the effective cationic charge and q is the occupation number of the d^q shell. The Racah parameter is well-expressed by the relation: B (cm⁻¹) = 384 + 58q + 124(z + 1) – 540 / (z + 1). The z value of cobalt is +1.103, considerably below the formal oxidation state (II) this reduction in oxidation state is suitable for M–N or M–O bonds [43]. Whereas, the value for nickel is –0.256, which reflects the overcoming of ligand anionic character on the nickel charge. The electronic spectra of two diamagnetic complexes, [Pd(Cl)₂(C₁₅H₁₄N₄O₂S)](H₂O) and [Pt(Cl)₂(C₁₅H₁₄N₄O₂S)](H₂O) are indicative for square-planar geometries (Fig. 2). Three spin-allowed singlet-singlet d-d transitions are anticipated for the geometry proposed. The ground states 1A_{1g}, 1B_{1g} and 1E_g are in order of increasing energy in low spin d⁸ systems. 1A_{1g} → 1A_{2g} (ν_1) and 1A_{1g} → 1B_{1g} (ν_2) transitions observed at ≈20,000 and 22,000 cm⁻¹ are characteristic for four arms surround the nucleus in planar state. Also, charge transfer bands observed in all investigated spectra in the range of 28,000–30,000 cm⁻¹ may assign for N → M and O → M bands. Intra-ligand transition bands expose to little shifted appearance around 31,000–35,000 cm⁻¹ attributed to n → π* and π → π* transitions.

3.4. X-ray diffraction

XRD patterns were carried out in the 10° < 2θ < 90° range for the free ligand and its complexes [Figs. 3, 2S] to give an apparent seeing about the lattice dynamics of solid compounds. The clear patterns exhibit the absence of contamination of starting materials. Known methods [44] were used to emphasize on the obscurity of peaks attributed to the reactants. All the patterns reflect comparatively nano-crystalline features for all compounds [45,46]. This may be attributed to the formation of a well-defined distorted crystalline structures. The θ , d values, full width at half maximum (FWHM) of prominent intensity peak, relative intensity (%) and particle size of compounds were existed in Table 5. The crystallite size was calculated by applying FWHM of the characteristic peaks using Deby–Scherrer equation: $B = 0.94 \lambda / (S \cos \theta)$, where S is the crystallite size, θ is the diffraction angle, B is

the line width at half maximum height, Cu/Kα (λ) = 1.5406 Å. The inner crystal plane d-spacing values were determined by using Bragg equation: $n\lambda = 2d\sin(\theta)$ at n = 1. The sizes calculated are distinguished in nanometer sized range (below 15 nm). The edge lengths of the particles for imaginative cubic shapes are as follow; 93.72(H₃L), 101.78(Co), 79.04(Ni), 79.11(Pd) and 70.03(Pt) Å.

3.5. Transmission electron microscopy

TEM has turn out as widely employed method for illustrating the particle shape and size. High resolution transmission electron micrograph images were extracted (Fig. 3S). The micrographs exhibit nanometer sized particles for Co(II) and Ni(II) complexes with diameter range 10.2–91.5 nm. The size determined for the ligand, Pd(II) or Pt(II) complexes display their presence in micro-scale. This appearance may refer to the aggregation for the particles which prohibit the exact determination. The images show the spherical shape as the main aspect except Pd(II) complex appears by rocky shape [37]. The spherical shape of nano-particles may be attributed to highly symmetric spherical chlorido groups introducing the complexation area. These topologies of the complexes pointed to the presence of metal ions have a significant influence on the formation of the nanometer particles [47]. The spherical shapes observed express that these morphologies are constituted by a distinct accumulation of several individual particles in polycrystalline nature. The aspect of moderately strong diffraction spots rather than diffraction rings confirms the formation of moderately single crystalline cube of complexes [48,49]. The dark areas in micrographs, are related to the high concentration of the particles naturally combined. The nanometer sized aspect may improve the properties in current application concerning the biological activity area with respect to bulk analogue. This feature may facilitate the penetration of particles inside the cell membrane. The out of comparison in-between the XRD and SEM results may clarify the difference between two techniques with the priority of XRD.

3.6. Thermal analysis

The plausible degradation behavior of all interested compounds over the stages was translated to the data displayed in Table 6. The Schiff base ligand was decomposed completely over three stages till reaching 550 °C with carbons residue. The degradation process for all investigated complexes was started at low temperature. The first step contributes to the removal of solvent molecules attached physically with the coordination sphere. The coordinating sphere starts its decomposition approximately with the first step which takes a broad range of temperature.

Table 10
Molecular docking energy values obtained for Schiff base ligand towards different receptors.

Receptor	Est. free energy of binding (kCal/mol)	Est. inhibition constant (K _i) (uM)	vdW + bond + desolve energy (kCal/mol)	Electrostatic energy (kCal/mol)	Total intercooled energy (kCal/mol)	Frequency	Interact surface
2ylh	–6.53	16.30	–8.38	–0.22	–8.60	30%	686.011
3t88	–4.92	246.46	–7.26	+0.05	–7.22	10%	721.741
3cku	–2.82	8.52	–4.67	+0.05	–4.62	10%	451.107
3ty7	–3.60	2.31	–5.30	–0.17	–5.47	10%	538.005
2jrs	–3.34	3.59	–5.74	–0.06	–5.80	30%	631.708

Table 11

The inhibition zone values (mm) against different microorganisms, for the ligand and its complexes.

Compound	Fungus		Bacteria	
	<i>Aspergillus flavus</i>	<i>Candida albicans</i>	<i>Escherichia coli</i> (G–)	<i>Staphylococcus aureus</i> (G+)
1)	10.7 ± 0.24	9.9 ± 0.34	16.7 ± 0.42	18.1 ± 0.41
2)	11.4 ± 0.36	10.7 ± 0.31	18.1 ± 0.48	14.6 ± 0.52
3)	10.8 ± 0.41	11.1 ± 0.43	18.9 ± 0.49	15.4 ± 0.45
4)	11.6 ± 0.36	10.9 ± 0.21	16.4 ± 0.35	12.7 ± 0.37
5)	10.2 ± 0.31	8.8 ± 0.24	16.7 ± 0.59	18.2 ± 0.44
Ampicillin	–	–	22	18
Norfloxacin	–	–	30	31
Amphotericin B	17	18	–	–

Sequential successive degradation process for all complexes through the stages up to 580 °C was followed. The residual part recorded includes free metal atoms, metal polluted with carbons or metal oxide. A slight difference was observed between the calculated and found weight losses in few degradation stages. This is due to the overlapping in-between follower steps which prohibit the exact determination for the step limits. This is affecting on calculating the thermodynamic parameters for all stages but choosing suitable ones have distinct limits.

3.7. Theoretical calculations

3.7.1. Kinetic studies

In order to emphasize on the influence of metal ion on the thermal behavior of the complex, the order n and the heat of activation E for defiant decomposition stages were calculated from the TG and DTG.

3.7.1.1. Coats–Redfern equation. The equation is an integral method, represented as:

$$\int_0^a \frac{da}{(1-a)^n} = \frac{A}{\phi} \int_{T_1}^{T_2} \exp\left(\frac{-E^*}{RT}\right) dt. \quad (5)$$

For convenience of integration the lower limit T_1 is usually taken as zero. This equation on integration gives:

$$\ln\left[\frac{-\ln(1-a)}{T^2}\right] = \ln\left(\frac{AR}{\phi E^*}\right) - \frac{E^*}{RT}. \quad (6)$$

A plot of $\ln\left[\frac{-\ln(1-a)}{T^2}\right]$ (LHS) versus $1/T$, E^* is the energy of activation in J mol^{-1} calculated from the slop and A is (S^{-1}) from the value of intercept (Fig. 4S). The entropy of activation ΔS^* in ($\text{J K}^{-1} \text{mol}^{-1}$) was calculated by using the equation:

$$\Delta S^* = R \ln\left(\frac{Ah}{K_B T_s}\right) \quad (7)$$

where K_B is the Boltzmann constant, h is the Plank's constant and T_s is the DTG peak temperature [23].

3.7.1.2. Horowitz–Metzger equation. Using derived relation [28] i:

$$\ln[-\ln(1-a)] = \frac{E}{RT_m} \theta \quad (8)$$

where a , is the fraction of the sample decomposed at time t and $\theta = T - T_m$.

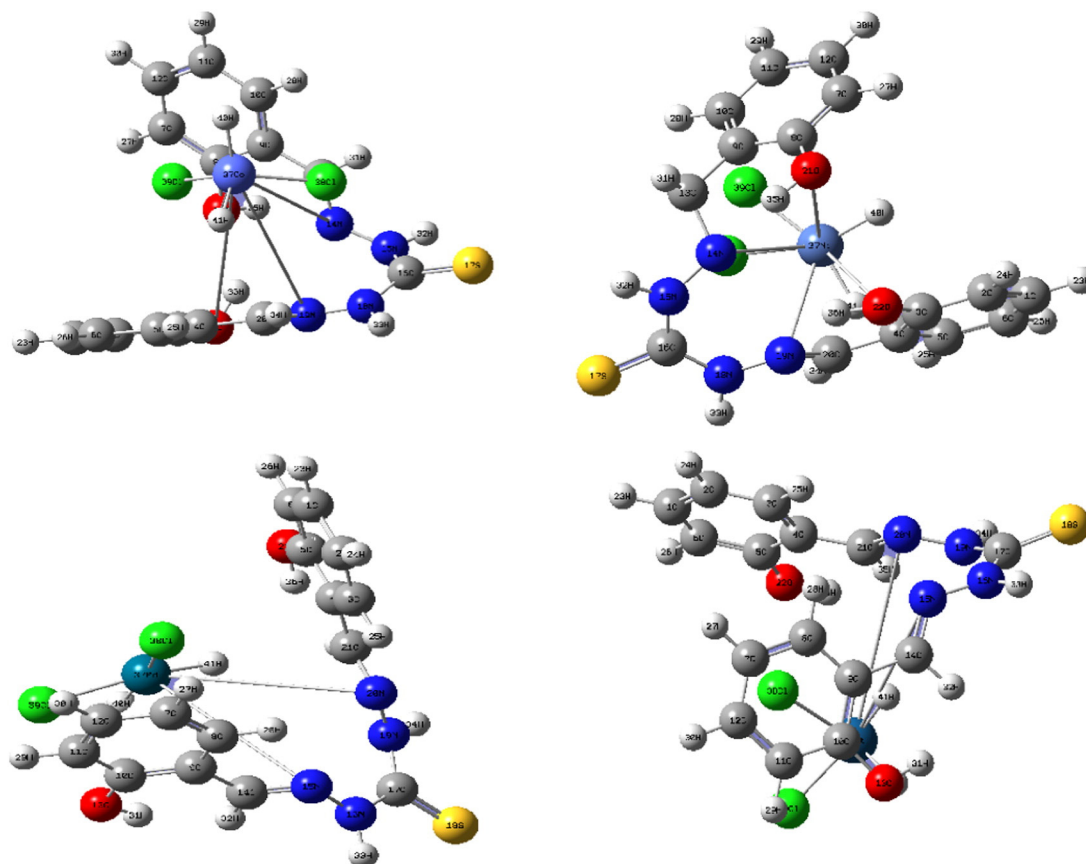


Fig. 2. The optimized structures for all complexes.

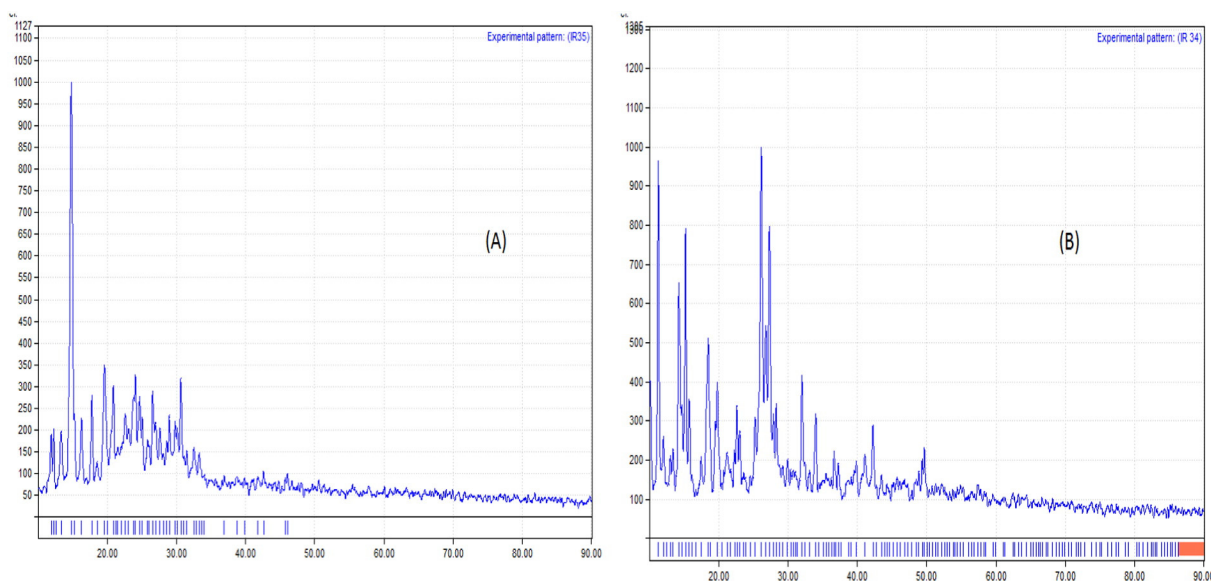


Fig. 3. X-ray patterns of Schiff base ligand (A) and Ni(II) complex (B).

Plot, $\ln[-\ln(1-a)]$ versus θ (Fig. 4S), was found to be linear, from the slope of which E , was calculated and Z can be deduced from the relation:

$$Z = \frac{E\varphi}{RT_m^2} \exp\left(\frac{E}{RT_m}\right) \quad (9)$$

where φ is the heating rate, the order of reaction, n , can be calculated from the relation:

$$n = 33.64758 - 182.295a_m + 435.9073a_m^2 - 551.157a_m^3 + 357.3703a_m^4 - 93.4828a_m^5 \quad (10)$$

where a_m is the fraction of the substance decomposed at T_m .

The enthalpy of activation ΔH^* and Gibbs free energy were calculated from using $\Delta H^* = E^* - RT$ and $\Delta G^* = \Delta H^* - T\Delta S^*$, equations. Also the entropy of activation ΔS^* was calculated from Eq. (7) and the data were tabulated (Table 7). The following observations were recorded: (i) the reduction for the activation energy (E) values for the second step in complexes TG, may reflect the weakness of intra-ligand bonds due to complexation (ii) the negative values of ΔS^* may indicate that the fragments have ordered structures which override along the complexes degradation (iii) the positive values of ΔH^* reflect the endothermic decomposition process, (iv) the positive values of ΔG^* reveal that the free energy of the decomposition residue is higher than that of the initial compound, and the decomposition stages are non-spontaneous. The upraising of $T\Delta S^*$ values (by negative single) than the ligand lead to override ΔG^* values which may reflect the lower rate of decomposition for the complexes [50].

3.7.2. Molecular modeling study

Gaussian09 Molecular Modeling for the free ligand and its metal ion complexes were implemented to abstract important quantum chemical parameters and optimized geometries. The frontier orbital energy gap between E_{HOMO} & E_{LUMO} is an important parameter used to characterize the electronic structure of molecules and also used to define their reactivity [51]. From the MO's images (Fig. 4), it can be seen that the HOMO and LUMO are mainly centered on N atoms of carbothiohydrazide moiety, which is considered the location for donor and acceptor atoms. Although, the LUMO level is also centered with Pd(II) and Pt(II) atoms, which considered the other acceptors of charge from HOMO level. Moreover, electronegativity (χ), chemical potential (μ),

global hardness (η), global softness (S), global electrophilicity index (ω) and the absolute softness (σ) were evaluated according to definite equations [52,53]. Electrophilicity index (ω) is one of the most important quantum chemical descriptors in describing toxicity and the reactivity of various selective sites. The electrophilicity may quantify the biological activity of drug receptor interaction. Also, this index measures the stabilization energy when the system acquires extra negative charge from the environment. η and σ indexes, are the measure of the molecular stability and reactivity also, their concepts are related to each others. The softness indexes are the vice versa image for global hardness [54].

3.7.2.1. Quantum chemical parameters. The calculated data presented in Table 8 reflect the following notes for the ligand in free state:

I) The molecule is having soft character with flexible donation towards the metal ions which reflects its reactivity. II) The positive electrophilicity index (χ) value and the negative electronic chemical potential (μ) value indicate that the molecule capable for accepting electrons from the environment and its energy must decrease upon accepting electronic charge. Therefore, the electrochemical potential must be negative.

The modeling calculations for complexes are displaying the following notice;

I) Small frontier orbital energy gaps (ΔE) were observed in comparing with the ligand value, may clarify the softness of complexes which reflect high expectation for biological reactivity. II) The E_{HOMO} values elevated from the free ligand may be accompanied with the elongated weak metal–ligand bonds. III) The dipole moment values ordered by: Co(II) > Ni(II) > Pt(II) > Pd(II). This may transpire the ionic interaction of donor sites with Co(II) ion than the others. This is considerably agrees with the spectral Racah parameter values for Co(II) and Ni(II) complexes.

3.7.2.2. The bond length and atomic charges. According to the numbering scheme given in the view (Fig. 2), the bond lengths over optimized geometries were calculated. Significant bond lengths were deduced and tabulated in Table 9. The coordinating groups (C=N and O=C) suffer an elongation than the original form of the ligand. Also, the coordinating sites have high charge density which qualify them for best coordination. Charges over free coordinating sites are; N(15) = -0.17623 , N(20) = -0.166195 , O(13) = -0.150877 and O(22) = -0.162303 . The approximately reduced charges over oxygen atoms before coordination, may refer to their participation in conjugation with phenyl groups or

presence of intra-ligand H-bonding. This may minimize their chance for coordinating approach with all metal ions. The oxygen sites are coordinating with Pd(II) and Pt(II) ions, so their effective charges are reduced only with these concerned complexes. Also, the two nitrogen charges were reduced after complexation. This is convenient with their participation in coordinating approach.

3.7.3. Molecular docking

Over the last decade, computational amplitude enhanced dramatically making possible to use more sophisticated and computationally intense methods in computer-encouraged drug design. The Autodock tools used to predict the biological features of candidate drug or emphasis on experimental results. This study interested in using defiant protein receptors attributed to microorganisms used in biological application. *Escherichia coli* (3t88, Crystal structure of *Escherichia coli* MenB in complex with substrate analogue, OSB-NCoA, Classification: lyase/lyase inhibitor), *Staphylococcus aureus* (3ty7, Crystal Structure of Aldehyde Dehydrogenase family Protein from *Staphylococcus aureus*, Classification: oxidoreductase), *Aspergillus flavus* (3cku, Urate oxidase from

aspergillus flavus complexed with its inhibitor 8-azaxanthin and chloride, Classification: oxidoreductase), *canadida albicans* (2ylh, structure of N-terminal domain of *Candida albicans* ALS9-2G299W mutant, Classification: cell adhesion) and *hepatocellular carcinoma* (2jrs, Solution NMR Structure of CAPER RRM2 Domain, Northeast Structural Genomics Target HR4730A, Classification: RNA binding protein) are the receptors docked with Schiff base ligand (inhibitor). The calculated energies for the docking process are listed in Table 10. The free energy of binding, inhibition constant, electrostatic energy, total intercooled energy and interact surface for receptor-inhibitor complexes were calculated. So, the reduction in binding energy due to mutation, will increase the inhibitor binding affinity towards protein receptors [55]. Also, these data introduce the best interaction stability for docked complexes (Fig. 5, 5S). According to computational calculation HB plot curves (Figs. 6, 6S) display different interaction degrees arranged by: 2jrs > 3t88 > 2ylh > 3ty7 > 3cku. This is referring to variable capability for H-bonding interaction inside the docked complexes. A distinguish inter-hydrogen bonding was appeared with 2jrs receptor-inhibitor complex. 2D-plot curves (Figs. 7, 7S) explain the mode of interaction inside the docking complex. The inhibitor thioamide

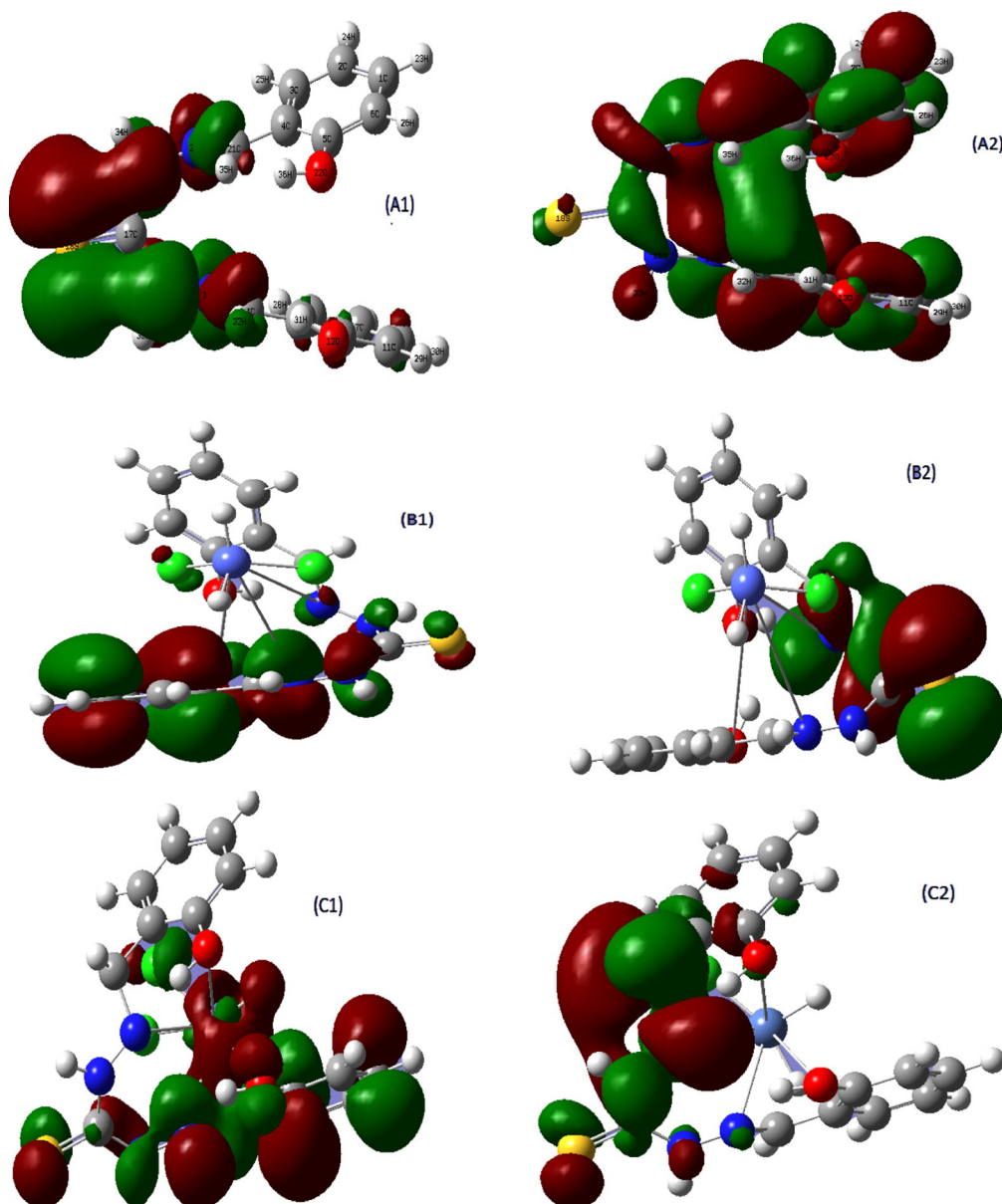


Fig. 4. The frontier molecular orbital's of HOMO(1) & LUMO(2) pictures of the optimized, ligand, Co(II), Ni, Pd(II) and Pt(II) complexes (A,B,C,D and E, respectively).

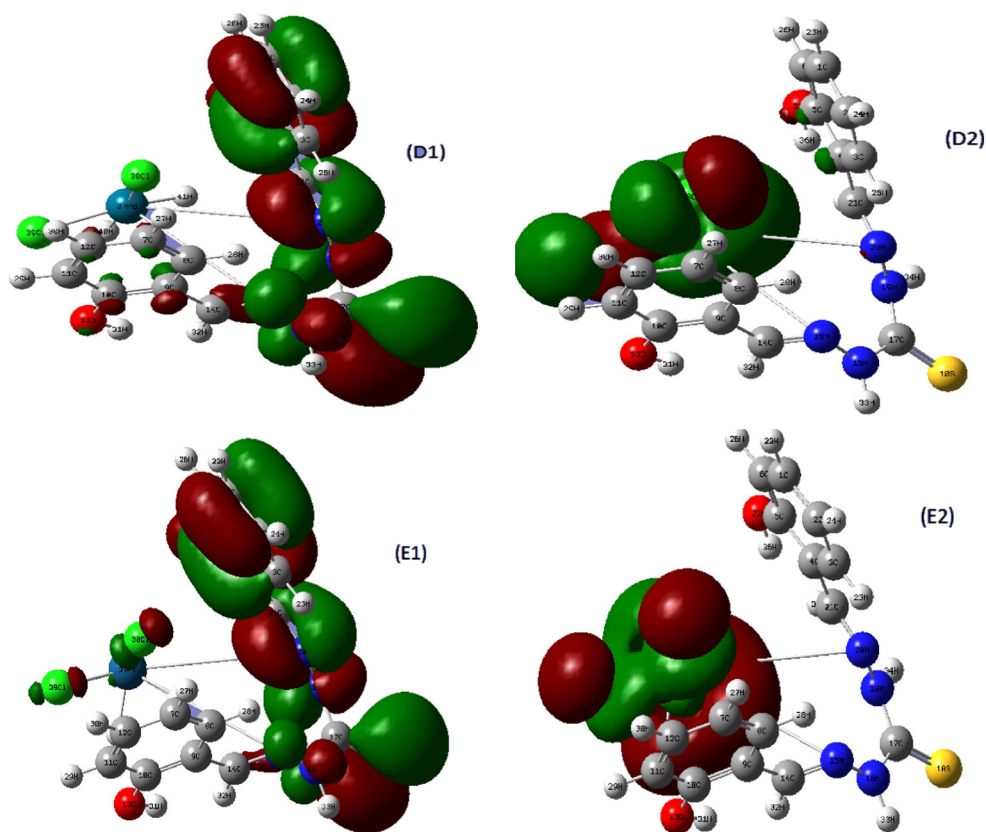


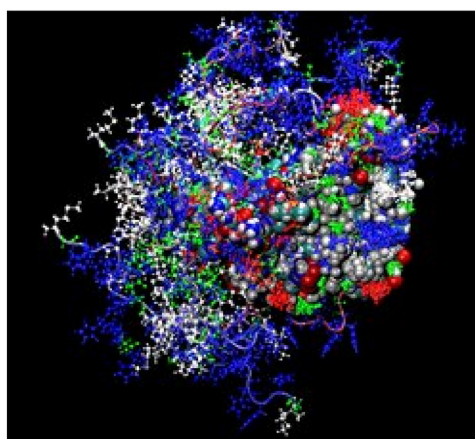
Fig. 4 (continued).

NH groups, are responsible for interaction with receptors. Finally the pharmacologically activity of the investigated Schiff base ligand was substantially anticipated.

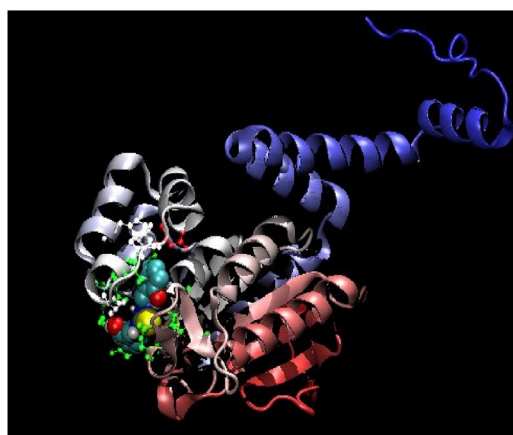
3.8. Biological activity

The biological investigation was carried out towards various microorganisms and the results were displayed in Table 11. The ligand and its complexes display significant inhibitory effect against all bacteria and fungi. Co(II) and Ni(II) complexes exhibit serious inhibition appeared with zone diameter (mm) nearby known drugs. This

drug-likeness effect may attribute to the reduction for metal ion charges which calculated previously. These reduced charges for central atoms enhance the lipophilicity of the complex inside the cell lipid. This lipid solubility facilitates the interaction of the compound with biological systems and blocking their active sites. The inhibition activity against hepatocellular carcinoma cells (Fig. 8) were recorded. The weak inhibition is the general trend appeared except for Co(II) and Ni(II) complexes. IC_{50} was determined for all complexes, in-between Co(II) and Ni(II) complexes have 18.8 and 36 μg values. These values interpret the significance effect of low concentration of such complexes against hepatocellular carcinoma cells.



(A)2jrs



(B)3t88

Fig. 5. Protein-inhibitor complexes for 2jrs and 3t88 receptors.

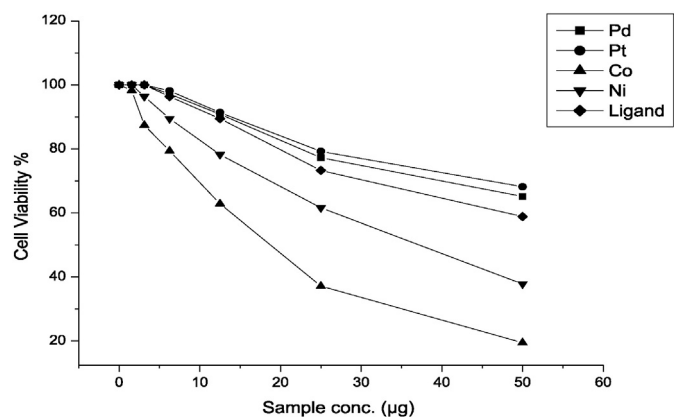


Fig. 8. The inhibition activity against hepatocellular carcinoma cells.

hepatocellular carcinoma cells. Co(II) and Ni(II) complexes are introducing a distinguish inhibition activity towards all microorganisms and offer the best IC_{50} values.

Appendix A. Supplementary data

Supplementary data to this article can be found online at <http://dx.doi.org/10.1016/j.molliq.2016.04.083>.

References

- [1] N.M. El-Metwaly, R.M. El-Shazly, I. Gabr, A.A. El-Asmy, Spectrochim. Acta A 61 (6) (2005) 1113.
- [2] N.M. El-Metwaly, I.M. Gabr, A.M. Shallaby, A.A. El-Asmy, J. Coord. Chem. 58 (13) (2005) 1154.
- [3] A.A. El-Asmy, N.M. El-Metwaly, G.A. El-Hazmi, Trans. Met. Chem. 31 (2006) 680.
- [4] A.A. Abou-Hussen, N.M. El-Metwaly, I.M. Saad, A.A. El-Asmy, J. Coord. Chem. 58 (18) (2005) 1735.
- [5] R.M. El-Bahnasawy, L.M. Sharaf El-Deen, A.S. El-Table, M.A. Wahb, A. El-Monsef, Abd El-Mense, Eur. Chem. Bull. 3 (5) (2014) 441–446.
- [6] M. Cindri, M. Rub, I. ilovi, G. Giester, B. Kamenara, Croat. Chem. Acta 80 (2007) 583–590.
- [7] N.M. El-Metwaly, I.M. Gabr, A.A. Abou-Hussen, A.A. El-Asmy, Transit. Met. Chem. 31 (2006) 71–78.
- [8] R.K. Shah1, K.S. Abou-Melha, F.A. Saad, T. Yousef, G.A.A. Al-Hazmi, M.G. Elghalban, A.M. Khedr, N.M. El-Metwaly1*, J. Therm. Anal. Calorim. 123 (1) (2016) 731–743.
- [9] N.M. El-Metwaly, A.A. El-Asmy, J. Coord. Chem. 59 (2006) 1591.
- [10] N.M. El-Metwaly, Transit. Met. Chem. 32 (2007) 88–94.
- [11] G.A. El-Hazmi, N.M. El-Metwaly, O.A. Al-Gamal, A.A. El-Asmy, Spectrochim. Acta A 69 (2008) 56–61.
- [12] N.M. El-Metwaly, khlood S. Abu-Melha, Transit. Met. Chem. 32 (6) (2007) 828–834.
- [13] K.S. Abou - Melha, N.M. El-Metwaly, Spectrochim. Acta A 70 (2008) 277–283.

- [14] A.A. El-Asmy, Y.M. Shaibi, I.M. Shediawa, M.A. Khattab, Synth. React. Inorg. Met. Org. Chem. 18 (1988) 231.
- [15] A.A. El-Asmy, I.M. Gabr, N.M. El-Metwaly, J. Coord. Chem. 61 (22) (2008) 3620–3633.
- [16] A.C. Scott, Laboratory control of antimicrobial therapy, in: J.G, et al., (Eds.), Practical Medical Microbiology, 13th ed. Churchill Livingstone, Edinburgh 1981, pp. 161–181.
- [17] T. Mosmann, J. Immunol. Methods 65 (1983) 55–63.
- [18] V. Gangdevi, J. Muthumary, Afr. J. Biotechnol. 6 (2007) 1382–1386.
- [19] A.P. Wilson, P. A, in: J.R.W. Masters (Ed.), Cytotoxicity and Viability Assays in Animal Cell Culture: A Practical Approach, third ed. Oxford University Press, 2000.
- [20] A.I. Vogel, Text Book of Quantitative Inorganic Analysis Longman, London, 1986.
- [21] G.A. Bain, J.F. Berry, J. Chem. Educ. 85 (2008) 532.
- [22] E.S. Freeman, B. Carroll, J. Phys. Chem. 62 (1958) 394–397.
- [23] W. Coats, J.P. Redfern, Nature 201 (1964) 68.
- [24] T. Ozawa, Bull. Chem. Soc. Jpn. 38 (1965) 1881–1886.
- [25] W.W. Wendlandt, Thermal Methods of Analysis, Wiley, New York, 1974.
- [26] J.H.F. Flynn, L.A. Wall, J. Res. Natl. Bur. Stand. A 70 (1996) 487.
- [27] P. Kofstad, Nature 179 (1957) 1362–1363.
- [28] H.W. Horowitz, G.A. Metzger, Anal. Chem. 35 (1963) 1464–1468.
- [29] X. Wu, A.K. Ray, Surf. Phys. Rev. B 65 (2002) 85403.
- [30] M.J. Frisch, et al., Gaussian 09, Revision D, Gaussian, Inc., Wallingford, CT, 2010.
- [31] R. Dennington II, T. Keith, J. Millam, GaussView, Version 4.1.1.2, Semichem Inc., Shawnee Mission, KS, 2007.
- [32] T.A. Halgren, J. Comput. Chem. 17 (5–6) (1998) 490–519.
- [33] G.M. Morris, D.S. Goodsell, et al., J. Comput. Chem. 19 (14) (1998) 1639–1662.
- [34] F.J. Solis, R.J.B. Wets, Research 6 (1) (1981) 19–30.
- [35] W. Geary, Coord. Chem. Rev. 7 (1971) 81–122.
- [36] K. Nakamoto, P.J. McCarthy, John WileyNewYork 1968.
- [37] Sawsan Al-Ashqer, Khlood S. Abou-Melha, G.A.A. Al-Hazmi, Fawaz A. Saad, Nashwa M. El-Metwaly, Spectrochim. Acta Part A 132 (2014) 751–761.
- [38] R.K. Shah, K.S. Abou-Melha, F.A. Saad, T. Yousef, G.A.A. Al-Hazmi, M.G. Elghalban, A.M. Khedr, N.M. El-Metwaly, J. Therm. Anal. Calorim. (2015), <http://dx.doi.org/10.1007/s10973-015-4838-z>.
- [39] Samy El-Megharbel, Nashwa El-Metwaly, Moamen Refat, Spectrochim. Acta A 149 (2015) 263–270.
- [40] M.B. Ferrari, S. Capacchi, G. Reffo, G. Aelosi, P. Tarasconi, R. Albertini, S. Pinellis, P. Lunghi, J. Inorg. Biochem. 81 (2000) 89.
- [41] A.B.P. Lever, Inorganic Electronic Spectroscopy, Elsevier, Amsterdam, 1986.
- [42] C.K. Jorgensen, Helv. Chim. Acta 50 (1967) 131–146.
- [43] R.T. Sanderson, Inorg. Chem., Reinhold, New York, 1967 (Chapter 6); H.J. Stoklosa, J. Chem. Educ. 50 (1973) 50.
- [44] B.D. Cullity, Elements of X-ray Diffraction, second ed. Wesley Inc., Addison, 1993.
- [45] A.A. Fahem, Spectrochim. Acta A 88 (2012) 10–22.
- [46] A. Shahrjerdi, S.S.H. Davarani, E. Najafi, M.M. Amini, Ultrason. Sonochem. 22 (2015) 382–390.
- [47] T. Yamanuchi, Y. Tsukahava, K. Yamada, T. Sakata, Y. Wada, Chem. Mater. 23 (2011) 75–84.
- [48] J.S. Ritch, T. Chivers, K. Ahmad, M. Afzaal, P.O. Brien, Inorg. Chem. 49 (2010) 1198; T. Mokari, M. Zhang, P. Yang, J. Am. Chem. Soc. 129 (2007) 9864–9865; J.J. Urban, D.V. Talapin, E.V. Shevchenko, C.B. Murray, J. Am. Chem. Soc. 128 (2006) 3248–3255.
- [49] B. Zhang, J. He, T.M. Tritt, Appl. Phys. Lett. 88 (2006) 043119; S.D. Robertson, T. Chivers, Dalton Trans. 1765 (2008).
- [50] S.S. Kandil, G.B. El-Hefnawy, E.A. Baker, Thermochim. Acta 414 (2004) 105–113.
- [51] I. Fleming, Frontier Orbitals and Organic Chemical Reactions, Wiley, London, 1976.
- [52] R.K. Ray, G.R. Kauffman, Inorg. Chem. Acta 173 (1990) 207–214.
- [53] R.C. Chikate, S.B. padhye, Polyhedron 24 (2005) 1689–1700.
- [54] S. Sagdinc, B. Köksöy, F. Kandemirli, S.H. Bayari, J. Mol. Struct. 917 (2009) 63–70.
- [55] S.K. Tripathi, R. Muttineni, S.K. Singh, J. Theor. Biol. 334 (2013) 87–100.